The neural chaperone proSAAS blocks α-synuclein fibrillation and neurotoxicity

Timothy S. Jarvela[a], Hoa A. Lam[b], Michael Helwig[a,1], Nikolai Lorenzen[c,2], Daniel E. Otzen[c], Pamela J. McLean[d], Nigel T. Maidment[b], and Iris Lindberg[a,3]

[a]School of Medicine, University of Maryland, Baltimore, MD 21201; [b]Department of Psychiatry and Biobehavioral Sciences, Semel Institute for Neuroscience and Human Behavior, University of California, Los Angeles, CA 90024; [c]Interdisciplinary Nanoscience Centre (iNANO), Department of Molecular Biology and Genetics, Aarhus University, DK-8000 Aarhus C, Denmark; and [d]Department of Neuroscience, Mayo Clinic, Jacksonville, FL 32224

Edited by Solomon H. Snyder, The Johns Hopkins University School of Medicine, Baltimore, MD, and approved June 14, 2016 (received for review January 20, 2016)

Emerging evidence strongly suggests that chaperone proteins are cytoprotective in neurodegenerative proteinopathies involving protein aggregation; for example, in the accumulation of aggregated α-synuclein into the Lewy bodies present in Parkinson's disease. Of the various chaperones known to be associated with neurodegenerative disease, the small secretory chaperone known as proSAAS (named after four residues in the amino terminal region) has many attractive properties. We show here that proSAAS, widely expressed in neurons throughout the brain, is associated with aggregated synuclein deposits in the substantia nigra of patients with Parkinson's disease. Recombinant proSAAS potently inhibits the fibrillation of α-synuclein in an in vitro assay; residues 158–180, containing a largely conserved element, are critical to this bioactivity. ProSAAS also exhibits a neuroprotective function; proSAAS-encoding lentivirus blocks α-synuclein-induced cytotoxicity in primary cultures of nigral dopaminergic neurons, and recombinant proSAAS blocks α-synuclein–induced cytotoxicity in SH-SY5Y cells. Four independent proteomics studies have previously identified proSAAS as a potential cerebrospinal fluid biomarker in various neurodegenerative diseases. Coupled with prior work showing that proSAAS blocks β-amyloid aggregation into fibrils, this study supports the idea that neuronal proSAAS plays an important role in proteostatic processes. ProSAAS thus represents a possible therapeutic target in neurodegenerative disease.

synuclein | proSAAS | chaperones | neurodegeneration | Parkinson's disease

Defects in neuronal proteostasis are at the center of a complex cause and effect cycle of neurodegenerative disease (reviewed in refs. 1–3). For example, in Parkinson's disease (PD), aberrant aggregation of the protein α-synuclein is thought to promote the production of toxic species, leading to repeated cycles of cellular toxicity (4). The neuropathological hallmark of PD is the presence of Lewy bodies, intracellular protein inclusions of which the main component is α-synuclein (5). Lewy bodies have also been found to contain various molecular chaperones: Hsp27, Hsp70 (6), clusterin (7), torsin A (6), and αB-crystallin (8). Protein chaperones support proteostasis in promoting proper protein folding, blocking aggregation, and facilitating the destruction of malformed proteins (9–11). There is increasing support for the idea that protein chaperones play an important role in the formation, deaggregation, and disposition of abnormal cellular aggregates in neurodegenerative disease (recently reviewed in refs. 2, 12, and 13).

The small secretory protein known as proSAAS (named after four residues in the amino terminal region) was originally discovered as an abundant peptide precursor in an unbiased mass spectrometric screen of brain peptides (14). Mammalian proSAAS, which is not glycosylated or phosphorylated (14), undergoes proteolytic cleavage at several pairs of basic residues, leaving a core region intact (15, 16); recent evidence shows that several processed peptides function as neuropeptides with specific receptors (17, 18). ProSAAS is expressed almost exclusively in neurons and neuroendocrine and endocrine cells, and it appears to be restricted to vertebrates (19–22). Although the C-terminal domain of proSAAS potently inhibits the proprotein convertase PC1/3 (23, 24), proSAAS distribution within the brain is far wider than that of PC1/3 (20, 21). ProSAAS and PC1/3 expression are also not coregulated (25, 26), supporting a broader array of neuronal functions for proSAAS beyond its interaction with PC1/3.

Interestingly, the proSAAS protein has been increasingly associated with the presence of neurodegenerative disease. Immunoreactive proSAAS has been identified in neurofibrillary tangles and plaques in brain tissue from patients with Alzheimer's disease, Pick's disease, and Parkinsonism–dementia complex (27, 28). In addition, four independent proteomic studies have found reduced levels of proSAAS-derived peptides in cerebrospinal fluid from patients with Alzheimer's disease (29–31) and frontotemporal dementia (32), suggesting possible brain sequestration. Recombinant proSAAS blocks $A\beta_{1-42}$ fibrillation in vitro, and proSAAS expression prevents the neurotoxic effects of $A\beta_{1-42}$ in cultured Neuro2A cells (33). Taken together, these data strongly suggest that the proSAAS sequence may contain specific elements that function as secretory antiaggregants in neurodegenerative disease. Given that proSAAS is a secretory protein, whether proSAAS could also function as an antiaggregant for cytosolic proteins prone to aggregation—such as α-synuclein—is not clear.

Significance

Aberrant protein homeostasis (proteostasis) is increasingly recognized as a major causal factor in the development of protein aggregates, including aggregation of α-synuclein in Parkinson's disease. Cellular proteins known as chaperones control proteostatic processes and are strongly associated with many different neurodegenerative diseases. We show here that an abundant brain- and endocrine-specific secretory chaperone known as proSAAS (named after four residues in the amino terminal region) exhibits potent antiaggregant effects on α-synuclein aggregation, and we identify a region of the protein that is necessary for this antiaggregant effect. We further show that proSAAS expression is able to stop α-synuclein from killing dopaminergic cells in a nigral cell model of Parkinson's disease. This work demonstrates an important role for the proSAAS protein in blocking aggregation in neurodegeneration.

Author contributions: T.S.J., M.H., N.T.M., and I.L. designed research; T.S.J., H.A.L., and M.H. performed research; N.L., D.E.O., and P.J.M. contributed new reagents/analytic tools; T.S.J., H.A.L., M.H., and N.T.M. analyzed data; and T.S.J., M.H., and I.L. wrote the paper.

The authors declare no conflict of interest.

This article is a PNAS Direct Submission.

[1]Present address: German Centre for Neurodegenerative Diseases (DZNE), 53175 Bonn, Germany.

[2]Present address: Large Protein Biophysics & Formulation, Novo Nordisk A/S, DK-2760 Malov, Denmark.

[3]To whom correspondence should be addressed. Email: ILindberg@som.umaryland.edu.

This article contains supporting information online at www.pnas.org/lookup/suppl/doi:10.1073/pnas.1601091113/-/DCSupplemental.

www.pnas.org/cgi/doi/10.1073/pnas.1601091113

In the study described below, we demonstrate that proSAAS is indeed a potent antiaggregant for α-synuclein, blocking its neurotoxicity; we show its association with Lewy bodies in the substantia nigra (SN) of patients with PD; and we identify a peptide region that is critical to its antifibrillation effect.

Results

ProSAAS Colocalizes with α-Synuclein–Rich Lewy Bodies Within the Human Substantia Nigra. To determine whether proSAAS localizes to Lewy bodies, we examined a human brain slice containing the SN from a patient with PD compared with a healthy control sample. In the healthy brain, proSAAS-immunoreactivity (ir) was diffusely distributed throughout the SN, with few incidences of punctate proSAAS-ir (Fig. 1 *A* and *B*). By contrast, in the sample from the patient with PD, proSAAS-ir was found in large concentrations throughout the SN (Fig. 1 *C* and *D*). These regions of high proSAAS-ir correlate with α-synuclein-ir. The α-synuclein-ir is found in cells that are stained by anti-MAP2 antibody, a marker for neuronal cell bodies and dendrites (Fig. 1*E*). Further, these regions of high α-synuclein-ir correspond to protein aggregates, as they colocalize with both p62, a marker for polyubiquitinated aggregates in Lewy bodies (Fig. 1*F*), and the aggregation-specific α-synuclein antibody 5G4 (Fig. 1*G*). Similar results were obtained using two other fixed samples of PD and control SN tissue obtained from the NIH NeuroBioBank [University of Maryland, Baltimore (UMB)]; Fig. S1 shows data from a second set of donors, as well as staining validation through the use of other proSAAS antisera.

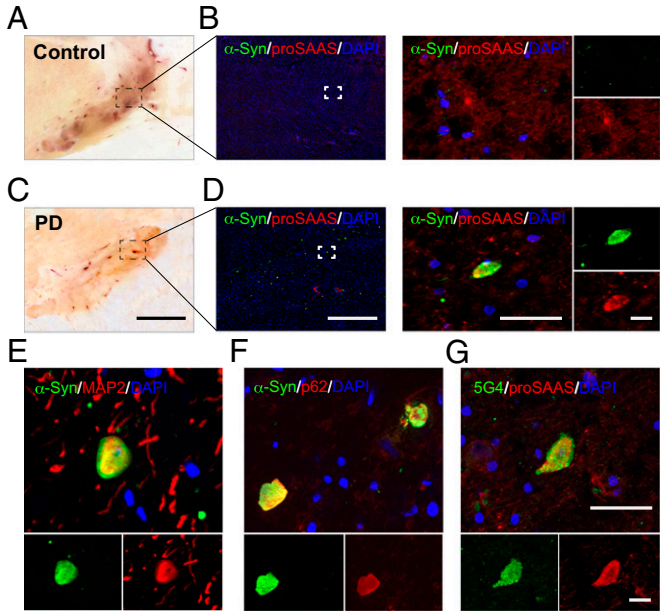

Fig. 1. Distribution of proSAAS immunoreactivity in control and PD SN. (*A* and *C*) Gross pathology of one representative healthy control (*A*) and PD case (*C*), demonstrating depigmentation of the SN compared with non-diseased control. (*B*) Immunohistochemical detection of α-synuclein revealed no significant deposits in the control samples. ProSAAS-ir (red) was detected throughout the extent of the human mesencephalon at the level of the SN. (*D*) Lewy bodies were detected within the SN in the PD patient sample. Low magnification images provide an overview of α-synuclein-ir deposits in Lewy bodies (green) and proSAAS expression (red). High magnification images of a representative Lewy body within the SN confirm a high degree of colocalization of proSAAS-ir with α-synuclein-ir. (*E*) Neuronal expression of α-synuclein within Lewy bodies was confirmed by colocalization of α-synuclein (green) with neuron-specific cytoskeletal protein MAP2 (red). (*F*) Colocalization of α-synuclein (green) with p62, a protein that colocalizes with ubiquitinated protein aggregates, indicates proteinopathy within Lewy bodies. (*G*) proSAAS (red) is associated with α-synuclein aggregates within Lewy bodies as detected by the antiaggregation-specific α-synuclein antibody 5G4 (green). [Scale bar: (*A* and *C*) 5 μm; (*B* and *D*) low, 1,000 μm; mid, 40 μm; and high, 20 μm.]

ProSAAS Dose-Dependently Inhibits α-Synuclein Fibril Formation. As proSAAS immunoreactivity was found to colocalize with Lewy body α-synuclein, we next sought to determine if recombinant proSAAS might affect α-synuclein fibrillation. Highly purified α-synuclein was incubated with varying concentrations of purified recombinant 21-kDa proSAAS (proSAAS 1–180) (Fig. 2*A*), the proSAAS domain preceding the second furin consensus cleavage site at residues 181–184 (14); this site is known to be quantitatively cleaved in vivo (15, 16). The effect of proSAAS on α-synuclein fibrillation was determined by monitoring the fluorescence intensity of thioflavin T (ThT), a fluorescent dye that increases in emission by several orders of magnitude after binding to amyloid fibrils (34). Within a given experiment, the half-time for fibrillation of α-synuclein alone, with a negative control protein (carbonic anhydrase) or varying concentrations of proSAAS (0.1–3.0 μM) ranged between 57 and 67 h (Fig. 2*A*). At ∼125 h, ThT fluorescence began to level off for all conditions. The total amount of fibrillation in wells treated with 1.0 μM or higher concentrations of proSAAS was significantly decreased compared with α-synuclein treated with buffer only, or to α-synuclein treated with the globular control protein carbonic anhydrase (chosen on the basis of similar size) ($P < 0.005$, two-way ANOVA). Of note, α-synuclein was present at a concentration of 70 μM; the effective protection ratio of proSAAS is therefore 1:70 proSAAS:α-synuclein. Interestingly, increasing concentrations of proSAAS appeared to change the kinetics of α-synuclein fibrillation by decreasing lag time (2.0 and 3.0 μM proSAAS, 40 h, $P < 0.05$).

We next tested whether proSAAS addition could affect preformed fibrils. Purified proSAAS or carbonic anhydrase was added at a 2-μM final concentration to fibrils in fibrillation assays that had plateaued. ProSAAS addition did not cause a decrease in ThT fluorescence [not significant (n.s.), $P > 0.05$] relative to preaddition levels or to the carbonic anhydrase control (Fig. 2*B*), indicating that proSAAS does not function as a disaggregase, nor does it displace ThT binding.

ProSAAS Residues 97–180 Are Sufficient to Prevent α-Synuclein Aggregation; Residues 158–180 Are Critical. Various truncated proteins were tested for potency against α-synuclein fibrillation. Truncation constructs were designed based on the predicted secondary structure (Fig. 3*A*). ProSAAS truncated variants were purified and subjected to the α-synuclein fibrillation assay (Fig. 3 *B* and *C*). Deletion of the N-terminal–most region of proSAAS had no effect on the potency of proSAAS against α-synuclein fibrillation (Fig. 3*C*), as 2.0 μM of proSAAS 1–180 and 97–180 were equally effective at preventing α-synuclein fibrillation ($P < 0.001$). The deletion construct proSAAS 62–180 was more effective in blocking α-synuclein fibrillation than either 1–180 or 97–180; this may be due to its improved solubility. In contrast, deletion of amino acids 158–180 strongly reduced the protective effect of proSAAS on α-synuclein fibrillation (Fig. 3*C*), demonstrating that this relatively conserved region (22) is critical to its antiaggregant properties. The known lens chaperone α-crystallin (2 μM) was used as a positive control. In separate experiments, the final product of fibrillation was assessed by centrifugation and SDS/PAGE to determine extent of fibrillation. In these experiments, the majority of α-synuclein remained in the supernatant for both proSAAS 1–180 and α-crystallin, but proSAAS 1–157 caused the majority of α-synuclein to pellet (Fig. 3 *D* and *E*).

ProSAAS Does Not Protect Against Intracellular Oligomerization of α-Synuclein in Cell Culture. A growing consensus in PD pathology indicates that the smaller oligomers rather than the larger aggregates represent the toxic species of misfolded α-synuclein (4). To test the ability of proSAAS to block the initial oligomerization of α-synuclein, we used a cell-based split-Venus complementation

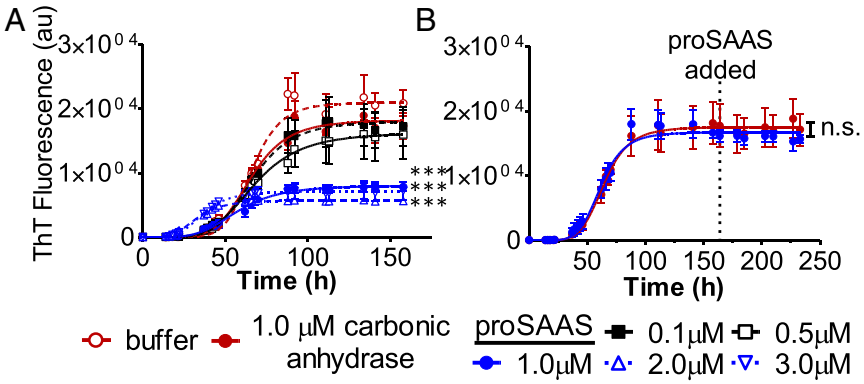

Fig. 2. ProSAAS blocks the fibrillation of α-synuclein in a dose-dependent manner. (*A*) α-Synuclein (70 μM) was subjected to fibrillating conditions in the presence of vehicle; a negative control protein, carbonic anhydrase (1 μM); or increasing concentrations of 21-kDa proSAAS (0.1, 0.5, 1.0, 2.0, and 3.0 μM). Each point is represented by the mean ± SEM, $n = 6$. (***$P < 0.001$, two-way ANOVA, vs. vehicle-only control). (*B*) Addition of proSAAS (1 μM) or the negative control protein carbonic anhydrase (1 μM) to preformed fibrils does not disrupt fibrils. ProSAAS or carbonic anhydrase were added to wells of fibrillated α-synuclein after fibrillation had leveled off at 172 h; fibrillation was monitored for an additional 72 h. There was no change in ThT fluorescence in either condition (n.s. $P > 0.05$, two-way ANOVA). Each point represents the mean ± SEM, $n = 4$.

assay (35, 36) and quantified oligomerization in SH-SY5Y cells. Importantly, this assay may not distinguish between native or misfolded oligomers, although the maturation time required to form the Venus fluorophore suggests that a very stable interaction is required, on the order of hours (37). Cells that were transiently transfected with both halves of the split-Venus α-synuclein constructs and cultured in media with added buffer, 1 μM ovalbumin, or 1 μM proSAAS for 24 h, showed an increased level of Venus fluorescence compared with cells transfected with LacZ-encoding constructs (Fig. 4*A*). Unexpectedly, the total levels of Venus fluorescence were significantly increased in wells treated with proSAAS compared with those treated with buffer or ovalbumin ($P < 0.05$). However, when individual cells on coverslips were analyzed by confocal microscopy, there was no significant difference in fluorescence levels between treatment conditions. These data suggest that the increase in total well fluorescence is due to changes in cell number rather than changes in α-synuclein oligomerization. When plate data were corrected for cell number using the water-soluble tetrazolium (WST1) cell proliferation assay, no differences were seen in the level of intracellular Venus fluorescence (Fig. 4*B*), indicating that added recombinant proSAAS does not affect intracellular synuclein oligomerization. This difference disappeared when cell expression of α-synuclein was lower and cell death was not observed, in which case cells incubated with proSAAS showed equal fluorescence to vehicle-treated cells (Fig. 4*C*). When cells were treated with the positive control (50 nM geldanamycin, an HSP90 inhibitor), the total Venus fluorescence was decreased to background levels.

ProSAAS Provides Protection Against α-Synuclein–Induced Cytotoxicity in SH-SY5Y Cells and Rat Primary Dopaminergic Nigral Cell Cultures. We then directly tested whether recombinant proSAAS can block α-synuclein–induced cytotoxicity in a cell culture overexpression system. SH-SY5Y neuroblastoma cells, which represent a dopaminergic cell model (38), were transfected with the complementary α-synuclein expression vectors discussed above or a control LacZ vector, split into wells of a 96-well plate, and grown in the presence of either a buffer-only control, 1 μM ovalbumin control, or 1 μM 21-kDa proSAAS. After 48 h, the percentage of surviving cells was calculated using the WST1 assay (Fig. 5*A*). α-Synuclein–transfected cells treated with a buffer control or ovalbumin showed a significant decrease in survival rates to 80% compared with LacZ-transfected controls ($P < 0.001$). When α-synuclein–exposed cells were treated with proSAAS, survival rates increased to 90% of the LacZ controls ($P < 0.01$), significantly higher than cells treated with only buffer or with the control protein ovalbumin ($P < 0.05$). Tunicamycin-induced cell death was not affected by proSAAS addition (Fig. S2*A*), nor was H_2O_2-induced cell death affected (Fig. S2*B*), indicating that proSAAS-mediated rescue is specific for α-synuclein–mediated cytotoxicity.

We next asked whether proSAAS could reduce the cytotoxicity associated with virally mediated α-synuclein overexpression in primary nigral cell cultures plated on a glial bed. Lentiviral proSAAS expression, rather than purified protein, was used to ensure a high level of proSAAS expression throughout the 7-d-long experiment. Primary cultures of 1- to 3-d postnatal rat substantia nigra (SN) were infected with α-synuclein–encoding adeno-associated virus (AAV), before plating (3 μL of 1×10^{12} transforming units per milliliter of AAV2/1), alone or in the presence of 3 μL of either proSAAS-encoding or eGFP-encoding lentivirus (4.2×10^{10} and 3.3×10^{10} copies per milliliter, respectively). Virus was added before plating on the glial bed to minimize dilution to the feeder layer. The number of surviving dopaminergic neurons (which we have previously shown make up ∼5% of total neurons in our nigral cultures) was determined by tyrosine hydroxylase (TH) staining 7 d later. Control conditions included untreated cultures, cultures infected with GFP-encoding AAV alone, and cultures treated with proSAAS-encoding lentivirus alone. One-way ANOVA revealed a significant effect of treatment group ($F_{5,26} = 4.56$, $P < 0.005$). Further analysis of differences between groups was conducted using Student's t test on planned comparisons. Cultures infected with α-synuclein–encoding AAV had significantly fewer TH^+ cells compared with those infected with GFP-AAV ($P = 0.025$), demonstrating the expected toxicity of α-synuclein (Fig. 5*B*). This effect of α-synuclein was prevented in cultures simultaneously infected with proSAAS- but not eGFP-encoding lentivirus ($P = 0.04$) (Fig. 5*B*). Neither proSAAS-encoding lentivirus nor GFP-encoding AAV had any significant effect alone, compared with untreated cultures (Fig. 5*B*). The reproducibility and dose dependency of this proSAAS effect was assessed in a separate experiment (Fig. 5*C*). Again, the overall effect of treatment group in this experiment was demonstrated by one-way ANOVA ($F_{4,20} = 10.82$, $P < 0.0001$), and individual group differences were assessed by t test. In this case, α-synuclein expression more strongly reduced the number of surviving TH^+ neurons compared with untreated cultures ($P = 0.0004$). This effect was significantly attenuated by simultaneous application of proSAAS-encoding lentivirus at doses of both 3 μL and 1 μL of 4.2×10^{10} copies per milliliter ($P = 0.0005$ and $P = 0.01$, respectively). The number of surviving TH^+ cells was significantly different between the two doses ($P = 0.04$).

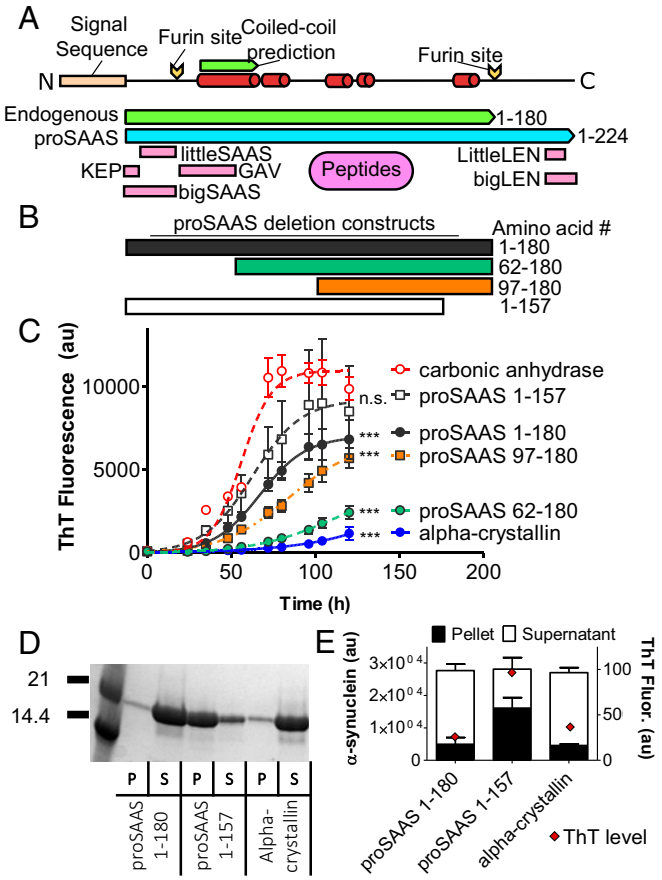

Fig. 3. Structure–function analysis of proSAAS on blockade of α-synuclein fibrillation reveals residues 158–180 are a critical determinant. (*A*) Illustration of proSAAS predicted secondary structure and notable features. α-Helices are in red, furin cleavage sites are shown in yellow, and known peptides are depicted in pink. (*B*) Diagram of His-tagged proSAAS deletion constructs. (*C*) A representative experiment of α-synuclein fibrillation inhibition by 21-kDa proSAAS and various proSAAS truncated proteins (proSAAS 1–157, 62–180, and 97–180). Each point is represented by the mean ± SEM, (***$P < 0.001$, two-way ANOVA, Bonferroni posttests compared with carbonic anhydrase control, $n = 6$ for each condition). (*D*) Coomassie gel of the supernatant (S) and pellet (P) fractions after centrifugation of plateaued fibrillating synuclein incubated either with proSAAS 1–180, proSAAS 1–157, or α-crystallin. (*E*) Quantification of the ratios between the supernatant and pellet fractions of two independent replicates (mean ± SEM). Corresponding average ThT values are marked in red (*Right y* axis). ThT fluorescence is shown as 1×10^{-2}.

These primary cell data provide additional support for the idea that proSAAS is cytoprotective against α-synuclein cytotoxicity.

Discussion

Chaperone proteins are increasingly recognized as important contributors to neuronal proteostasis (10, 12). Overexpression or exogenous addition of a variety of chaperone proteins is efficacious in delaying or preventing amyloid fibril generation both in in vitro and, more recently, in vivo models of various amyloidogenic diseases (39–41). However, the chaperones tested to date are ubiquitously expressed, and thus far no neuron-specific chaperone protein has been shown to have antiaggregant activity against amyloidogenic diseases such as PD. Because neurons are known to be particularly susceptible to secretory stress (42), neurally expressed chaperones are particularly well suited to play unique roles in neurodegenerative disease. In this report, we provide evidence that the neural protein proSAAS represents a potent antiaggregant chaperone against α-synuclein.

ProSAAS Is Diffusely Expressed in Neurons in Nondiseased Controls and Colocalizes with Lewy Bodies in PD. ProSAAS is a small secreted protein that is widely expressed within neurons, neuroendocrine cells, and endocrine cells (20, 21). ProSAAS is unusually abundant within the brain: the NIH GEO Profiles database indicates that proSAAS mRNA is in the top 1% of brain messages. Our immunohistochemical data show that normal human SN exhibits diffuse neuronal proSAAS staining. However, in nigral sections obtained from three different patients with PD, proSAAS staining was concentrated within Lewy bodies, suggesting possible cosequestration with α-synuclein during the α-synuclein aggregation process.

We found that recombinant proSAAS is a potent α-synuclein antiaggregant in vitro, blocking the production of fibrils even at a highly substoichiometric molar ratio of 1:70 proSAAS to α-synuclein. ProSAAS was previously shown to be effective at blocking $A\beta_{1-42}$ fibrillation at an effective ratio of 1:22 proSAAS:$A\beta_{1-42}$ (33) and also blocks the aggregation of human islet β-cell peptide islet amyloid polypeptide (43). Other protein chaperones such as Hsp70 (44, 45) and CsgC (46) have been used at molar ratio, 1:10 chaperone:α-synuclein. Like other non–ATP-dependent chaperones (47), proSAAS cannot disaggregate preformed fibrils, either of α-synuclein (Fig. 2*B*) or $A\beta_{1-42}$ (33). Interestingly, the addition of higher concentrations of proSAAS resulted in a small but significant decrease in lag time and *T*1/2 of the fibrillation reaction (Fig. 2*A*, 2 μM and above concentrations). We speculate that at high concentrations, proSAAS may lower lag time by diverting the fibrillation reaction to a nonfibrillar aggregative process; EM analysis could confirm this idea. Taken together, these data show that proSAAS is a highly effective protein chaperone that can prevent the fibrillation of aggregation-prone proteins, but cannot disaggregate already-formed fibrils.

ProSAAS Structure–Function Studies: Importance of Residues 158–180. ProSAAS was originally identified as a neuroendocrine peptide precursor (14) and is known to be naturally cleaved at two internal furin consensus sites as well as at several pairs of basic residues within its N- and C-terminal regions to generate bioactive peptides, leaving an internal unprocessed core (15, 16). Whereas mammals show >85% overall primary sequence conservation of proSAAS, conservation greatly decreases in nonmammalian vertebrates; *Xenopus* and zebrafish proSAAS exhibit only 29% and 30% overall identity with mouse proSAAS (22). Various secondary structure prediction algorithms support the likely presence of several short α-helices as well as a coiled-coil domain (Fig. 3*A*). Four stretches of moderate sequence conservation are apparent, with two forming parts of predicted α-helices. When we removed the conserved, carboxy-most α-helix from 21-kDa proSAAS (an abundant species naturally produced by cleavage at the second furin consensus site (residue 184) (15, 48), the protein lost its ability to block the fibrillation of α-synuclein. This finding suggests that this helix, ELLRYLLGRIL (Fig. S3) (residues 158–169 within mouse proSAAS) plays an important role in the chaperone activity of proSAAS. The fact that a well-conserved region within proSAAS (the 158–180 segment) is critical to its α-synuclein antifibrillation action supports the idea that this region is essential to its chaperone function.

What Is the Mechanism of proSAAS Protection Against α-Synuclein Cytotoxicity? At first glance, proSAAS does not appear to be a likely candidate to provide protection against α-synuclein–induced cytotoxicity. ProSAAS is a secreted protein that normally resides within the secretory pathway and/or extracellular space. By contrast, α-synuclein is a cytosolic protein, enriched at cytosol/membrane interfaces (49). However, α-synuclein has been identified in extracellular fluids in patients with PD and normal subjects (50–53). Further, extracellular secretion of α-synuclein is increased under conditions of cellular stress (54); and α-synuclein can also be

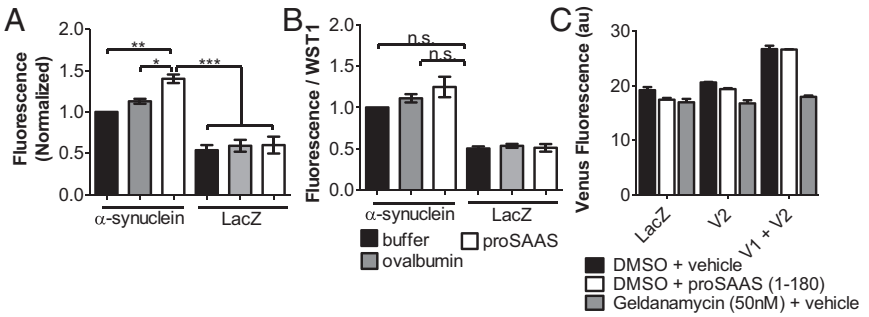

Fig. 4. Recombinant proSAAS does not block intracellular α-synuclein oligomerization. (*A*) Wells containing proSAAS-treated, α-synuclein–expressing cells show a significant increase in total Venus fluorescence over cells treated with ovalbumin or buffer. SH-SY5Y cells were transfected with either split Venus–α-synuclein cDNAs or pcDNA3.1-LacZ (negative control); buffer, proSAAS, or ovalbumin were added 48 h later, and Venus fluorescence was then measured (mean ± SEM, $n = 3$ independent experiments, more than six replicates in each experimental condition). Statistical significance was determined with one-way ANOVA analysis ($F = 41.98$) and Tukey's post hoc test. (*B*) Normalization of fluorescence to cell number. Once Venus fluorescence is normalized to the total number of living cells, the differences between proSAAS and buffer/ovalbumin negative controls are eliminated (mean ± SEM, $n = 3$ independent experiments, more than six replicates in each experimental condition). One-way ANOVA analysis ($F = 29.20$) and Tukey's post hoc test. (*C*) Venus fluoresecence at lower synuclein expression levels shows no difference between vehicle- and proSAAS-treated wells. Cells were transfected with both split-Venus constructs (V1 + V2). When treated with 50 nM geldanamycin, Venus fluorescence remained at background levels, comparable to LacZ- or V2-only transfected cells. $***P < 0.001$, $**P < 0.01$, $*P < 0.05$, n.s. $P > 0.05$.

released in a calcium-dependent manner via exosomes (55). Both monomeric and oligomeric forms of α-synuclein are present within vesicles and have been found extracellularly (56). We speculate that secreted proSAAS may interact with α-synuclein secreted into the extracellular space, where its concentration has been estimated to be subnanomolar (57). Extrapolation of published wet weight data indicates that brain concentrations of proSAAS range from 0.01 μM (cerebellum) to 0.5 μM (hypothalamus) (15, 48), supporting the idea of effective extracellular concentrations for this chaperone. Because secreted α-synuclein can undergo endocytosis (58) and enter neighboring cells (59), this may represent the pathway by which a putative proSAAS–α-synuclein complex enters the cell, generating the colocalization that we observed in cells within the substantia nigra of a patient with PD (Fig. 1). This idea is supported by our finding that externally added recombinant proSAAS can be internalized (Fig. S4). However, proSAAS was ineffective at blocking intracellular oligomerization of α-synuclein overexpressed in cell culture, as indicated by its lack of disruption of split-Venus α-synuclein complementation (note that the addition of the HSP90 inhibitor geldanamycin successfully reduced Venus fluorescence (Fig. 4*C*), suggesting that complementation fluorescence indeed arose from misfolded α-synuclein oligomers rather than from the formation of native tetramers). Additional work is necessary to determine the initial site of the proSAAS–synuclein interaction, for example, by determining whether secretion of α-synuclein is required for cytoprotection and assessing whether uptake of secreted α-synuclein and proSAAS can occur as a complex.

Although the fact that tunicamycin- or hydrogen peroxide-mediated cytotoxicity was not affected by proSAAS addition supports the specificity of proSAAS-mediated protection for α-synuclein–induced cytotoxicity, the physiological mechanism

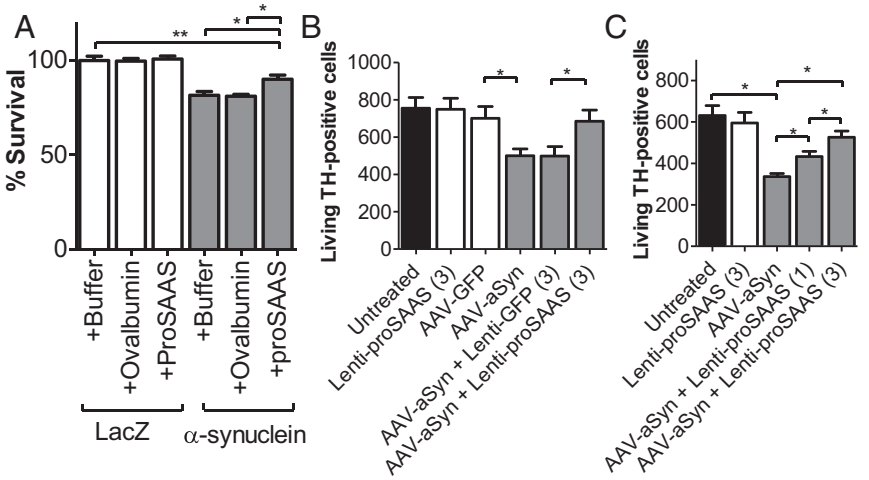

Fig. 5. ProSAAS blocks α-synuclein–induced cytotoxicity. (*A*) Addition of recombinant proSAAS blocks synuclein-mediated cytotoxicity in SH-SY5Y cells. Cells were transfected with α-synuclein–encoding constructs, split into 96-well plates, and treated with recombinant proSAAS or the control proteins shown. There was no significant difference between ovalbumin and buffer, but a significant difference exists between these two controls and all other conditions. $**P < 0.01$, $*P < 0.05$. Percent survival was determined by normalizing WST1 absorbance in each group to LacZ buffer-only control. Statistical significance was determined with one-way ANOVA analysis ($F = 27.13$) and Tukey's post hoc test. Average of three experiments with $n = 4$ replicates in each experiment. (*B*) Infection of rat primary nigral cells with a proSAAS-encoding lentivirus (3 μL of 4.2×10^{10} copies per milliliter) and (*C*) (1 or 3 μL of 4.2×10^{10} copies per milliliter) attenuates α-synuclein–induced neurotoxicity in two independent experiments. The number of TH^+ cells is shown on the *y* axis. $*P < 0.05$.

underlying proSAAS-mediated cytoprotection is not yet clear. The exact process by which α-synuclein kills dopaminergic cells is unknown, and it is likely that there are multiple contributing pathways. Overexpressed and/or mutant α-synuclein forms are especially toxic to dopaminergic cells (reviewed in ref. 60); indeed, previous experiments in our laboratory have shown the cytotoxic effect of viral-mediated α-synuclein to be selective to TH^+ cells in the nigral cultures. Oligomers are thought to represent the cytotoxic form (61). Overexpression and/or oligomerization of α-synuclein causes changes in membrane permeability (62), mitochondrial dysfunction (63), disruptions in endoplasmic reticulum/Golgi trafficking (64), lysosomal leakage (65), and impairment and inhibition of proteasomes (66, 67). Our finding of substoichiometric blockade of α-synuclein fibrillation, coupled with the demonstration of immunoreactive proSAAS within Lewy bodies, indicates that proSAAS could function upstream of cytotoxic processes by interacting with intracellular α-synuclein monomers in a transition state (68) that would otherwise propagate toward toxic fibril formation, or by interacting with oligomers to prevent further oligomerization, fibrillation, and cytotoxicity. However, as mentioned above, addition of extracellular proSAAS was ineffective in blocking intracellular α-synuclein oligomerization, although still attenuating cytotoxicity. We speculate that proSAAS may bind only to secreted forms of α-synuclein or bind to already-formed intracellular α-synuclein oligomers, reducing further growth. Alternatively, proSAAS might prevent the seeding of additional oligomers, perhaps through blocking of hydrophobic patches necessary for fibril formation. Once bound, proSAAS may blunt the toxic actions of α-synuclein in much the same way that antibody fragments against α-synuclein are able to prevent cytotoxicity (69).

In summary, we have here shown that the neurally expressed proSAAS chaperone is a potent antiaggregation agent that blocks α-synuclein fibrillation at very low molar ratios. Excess proSAAS, either delivered by increased synthesis/secretion (in primary nigral cells) or by addition of recombinant protein to growth media (in SH-SY5Y cells) provides specific protection against α-synuclein–mediated neurotoxicity. The present data support the idea that neuronal proSAAS plays an important chaperone role in protein aggregation in neurodegenerative disease and identify proSAAS as a potential therapeutic target in PD.

Materials and Methods

Reagents. The split-Venus α-synuclein constructs were made as described in ref. 39. Prokaryotic expression vectors containing mouse proSAAS 1–180, 62–180, and 97–180 were described previously (33). The pET45 proSAAS 1–157 construct was generated by GenScript by the insertion of a stop codon after nucleotide 471 in the insert (cctgacgtggaccctTAAgagctgc). α-Synuclein was purified according to procedures described previously (70), resuspended in water, filtered through a 0.22-μm syringe filter, and adjusted to a final concentration of 5 mg/mL. ProSAAS-encoding lentivirus (mouse) was prepared by GeneCopoeia, as previously described (33). The rabbit proSAAS antiserum, LS45, was raised against recombinant His-tagged proSAAS 1–180 (33); a purified IgG preparation obtained through Protein A chromatography was used here. This antiserum recognizes the various proSAAS truncated forms described below by both Western blotting as well as by ELISA, and exhibits 30% cross-reactivity with frog proSAAS (22). Antiserum LS45 has been previously used to demonstrate proSAAS immunoreactivity in pancreatic islets (71) and brains from patients with Alzheimer's disease (29). Deidentified human tissues were procured from the NIH NeuroBioBank. The University of Maryland Institutional Review Board and the Department of Veterans Affairs, Los Angeles obtained informed consent under preexisting protocols of UMB and Sepulveda Research Corporation, respectively.

Immunohistochemistry. Fresh-frozen human midbrain tissue samples containing the substantia nigra of a PD-affected male 75-y-old donor and non–PD-affected control tissue of a male 83-y-old donor were obtained from the Human Brain and Spinal Fluid Resource Center (managed by Sepulveda Research Corporation), a part of the NIH NeuroBioBank; data from these samples is shown in Fig. 1. Formalin-fixed samples of a different PD-affected male 79-y-old donor and non–PD-affected male 75-y-old control donor presented in Fig. S1 were received from the UMB Brain and Tissue Bank, also a part of NeuroBioBank. A third PD sample (from UMB; also formalin fixed) was also analyzed, with similar results. Coronal sections (20 μm) containing the SN were processed using a Thermo Scientific NX70 cryostat, collected on polysine object slides (Fisher Scientific) and (for fresh-frozen samples only) postfixed with 4% (wt/vol) paraformaldehyde for 10 min. Sections were then transferred into blocking solution (BS) containing 3% (wt/vol) BSA in 0.5% Triton X-100 in PBS (PBS-T) for 1 h to block nonspecific reactions. Before immunofluorescence staining, potential lipofuscin autofluorescence in the tissue sections was quenched using the TrueBlack Lipofuscin Autofluorescence Quencher (Biotium). Where appropriate, sections were then incubated with polyclonal rabbit anti-proSAAS protein A-purified IgG (LS45, 1:100 or 1:1,000) (33); antiserum LS44, 1:100 against SLSAASPLVETSTPLRL; a similar anti-SAAS peptide antiserum obtained from L. D. Fricker (14) at 1:1,000; monoclonal mouse anti–α-synuclein (clone 211, 1:500; BD Biosciences (72); mouse antiaggregated-α-synuclein (15G4, 1:500; Analytik Jena); polyclonal rabbit anti-MAP2 (ab24640, 1:200; Abcam); or guinea pig anti-p62 IgG (GP62-C, 1:150; Progen) in PBS overnight (4 °C). Sections were rinsed briefly in PBS and then incubated with the appropriate species-specific secondary antibodies DyLight488 (1:200, DI-2488 anti-mouse IgG; Vector Laboratories) and DyLight594 or Alexa Fluor 594 (1:200, DI-1594 anti-rabbit IgG; Vector Laboratories or A11076 anti-guinea pig IgG; Invitrogen) in PBS containing DAPI nuclear/DNA staining (5 ng/mL, D9542; Sigma-Aldrich) for 2 h at room temperature. Sections were rinsed in PBS and coverslipped with Vectashield mounting medium (Vector Laboratories). Fluorescence microscopy images were obtained using a Zeiss Observer.Z1 microscope (Carl Zeiss) equipped with a motorized stage. Low magnification overview images were generated with a 20× Plan-Apochromat objective (N.A. 0.8) followed by a computerized image stitching with ZEN 2 software (Carl Zeiss). For *z*-stack high-magnification imaging, stacks were collected at 2-μm intervals with a 63× Plan-Apochromat N.A. 1.4) objective using the same system, followed by deep focus postprocessing. Anatomical localization of immunoreactivity within the mesencephalon was annotated according to the Allen Human Brain Atlas (73) and Gray's Anatomy of the Human Body (30th Edition) (74).

Thioflavin T α-Synuclein Fibrillation Assay. The fibrillation of α-synuclein was measured by monitoring the fluorescence of thioflavin T (ThT) (Sigma-Aldrich) during incubation with proSAAS constructs and control proteins. A round bottom 96-well polypropylene dish (Falcon) was used to incubate all samples. Each well contained 100 μg α-synuclein, 10 μM ThT, 500 μM acetic acid, and PBS (pH 7.4) to a final volume of 100 μL. For testing proSAAS deletion constructs, 50 μg α-synuclein was used per well. ProSAAS and control proteins were added to the mixture at the concentrations noted in the figure legends in 5 mM acetic acid, a polytetrafluoroethylene 3/32-inch bead (McMaster-Carr) was added to each well, and foil-sealed plates were shaken in a rotary shaker at 300 rpm in a 37° incubator for the times indicated. Bottom-read fluorescence was measured at the times indicated using a SpectraMAX M2 spectrophotometer with an excitation peak at 450 nm and emission peak at 485 nm. Data were processed using GraphPad PRISM 5. Representative experiments are shown; all experiments were repeated at least twice with qualitatively similar results.

ProSAAS Purification. Plasmids encoding the various His-tagged proSAAS constructs were expressed in either XL1 Blue (proSAAS 62–180, 97–180) or BL21 (proSAAS 1–157, 1–180) bacteria. Bacterial cultures were incubated with shaking at 37 °C until an A_{600} of 0.6–0.8 was reached. Cultures were shifted to 26 °C and induced with isopropyl β-D-1-thiogalactopyranoside (Sigma-Aldrich) to a final concentration of 1 mM. Cultures were incubated with shaking overnight for 16 h. Bacteria were pelleted and the protein harvested using Bugbuster Protein Extraction Reagent (Millipore) according to the supplier's instructions. Clarified lysates were then applied to a 5-mL HisTrap HP column (GE Healthcare). The column was sequentially washed with 25 mL each of: 0.5 M NaCl, 20 mM Tris·HCl, 5 mM imidazole, pH 7.9; 0.5 M NaCl, 20 mM Tris·HCl, 60 mM imidazole, pH 7.9, all at 4 mL/min at 4 °C, before being eluted into 3-mL fractions with a total of 60 mL of 0.1 M NaCl, 20 mM Tris·HCl, and 1 M imidazole, pH 7.9 at 2 mL/min. Samples of each fraction were analyzed by SDS/PAGE and peak fractions were pooled and dialyzed into 3 L of ice-cold 0.1 M acetic acid overnight. Samples were then concentrated in Amicon Ultra centrifugal filter units (Millipore) with a 10-kDa molecular weight cut-off (MWCO) (proSAAS 1–180, 62–180, 1–157) or a 3-kDa MWCO (proSAAS 97–180) and resuspended iteratively in 5 mM acetic acid, for an effective 1,000-fold dilution. Proteins were centrifuged before use at 15,000 × *g*. Purified control proteins (ovalbumin, carbonic anhydrase, and α-crystallin; all from Sigma-Aldrich) were also dissolved in 5 mM acetic acid and adjusted to final working concentrations in this buffer. All proteins were over 90% pure, as estimated visually after Coomassie staining of 5 μg applied to Any kD SDS-polyacrylamide gels (Bio-Rad). Absorption at

280 nm (using calculated extinction coefficients) and QuikStart Bradford (Bio-Rad) protein assays were used to determine protein concentrations.

Split-YFP α-Synuclein Oligomerization Assay. SH-SY5Y cells were cultured in 50/50 DMEM/F12 media (HyClone; GE Healthcare) supplemented with 10% (vol/vol) FBS (Atlanta Biologicals) and 1% penicillin–streptomycin. Cells were split into 10-cm dishes and transfected with plasmids encoding split α-synuclein or control LacZ plasmid (75), using Continuum transfection reagent (Gemini Bio Products) following the manufacturer's protocol, with a DNA to transfection reagent ratio of 0.5 μg DNA/1.0 μL Continuum. The α-synuclein constructs contained the N-terminal half of Venus YFP fused with α-synuclein or the C-terminal half of Venus YFP fused with α-synuclein, as described previously (75). After 14 h, cells were split into a 96-well plate, and either proSAAS or ovalbumin was added at 1 μM final concentration or the equivalent volume of 5 mM acetic acid buffer ($n = 8$ for each condition). After 48 h, Venus fluorescence was measured with an excitation wavelength of 488 nm and emission wavelength of 540 nm with a cut-off at 530 nm using a SpectraMax M2 spectrophotometer (Molecular Devices) and the SoftMaxPro program, followed by a cytotoxicity measurement to normalize fluorescence to the number of living cells (see below). Representative experiments are shown; all experiments were repeated at least twice with qualitatively similar results.

SH-SY5Y Cytotoxicity Assay. For the α-synuclein toxicity assay, cells were transfected and incubated as previously described (see above). After 48 h, 10 μL of WST1 reagent (Roche) was added to each well of a 96-well plate and incubated for 3 h at 37 °C. The absorbance was then measured with a SpectraMax M2 spectrophotometer at 450 nm. Background absorbance was subtracted by calculating the absorbance at 650 nm. Where indicated, tunicamycin (Sigma-Aldrich) in ethanol was added to a final concentration of 5 μg/mL, concurrent with addition of either proSAAS to a final concentration of 1 μM or an equal volume of 5 mM acetic acid vehicle. The final concentration of ethanol never exceeded 1%. Where indicated, 100 μM H_2O_2 was added with proSAAS or acetic acid as previously described. Representative experiments are shown; all experiments were repeated at least twice with qualitatively similar results.

Primary Nigral Cell Culture α-Synuclein Cytotoxicity Assay. Primary cultures were prepared essentially as described by Sulzer et al. (76) with modifications to isolate nigral rather than ventral tegmental area cells. Procedures for isolation of brain tissue were approved by the University of California at Los Angeles Animal Care and Use Committee. Briefly, cultures were prepared in two stages. First, glia cultures were prepared from the cortex of 1- to 3-d-old postnatal rat pups. After a week, substantia nigra from 1- to 3-d-old postnatal rat pups were dissected and collected in cold phosphate buffer and digested in papain at 32 °C with oxygenation for 2 h. The tissue was dissociated by gentle trituration. The dissociated cells were incubated with combinations of AAV2/1 (3 μL of 1×10^{12} transforming units per milliliter encoding α-synuclein or GFP, and lentivirus encoding mouse proSAAS (33) or eGFP (1 or 3 μL of 4.2×10^{10} copies per milliliter and 3.3×10^{10} copies per milliliter, respectively), as described in *Results*, for 30 min at 37 °C, 5% (vol/vol) CO_2. Infected cells were plated on the established cortical glia bedding and incubated at 37 °C, 5% (vol/vol) CO_2 for 7 d. Cell cultures were fixed with 4% (wt/vol) paraformaldehyde for 15 min, washed with PBS, and incubated with 5% (vol/vol) normal donkey serum for 2 h at room temperature. Cells were labeled with 1:1,000 tyrosine hydroxylase antibody (EMD Millipore) and incubated overnight at 4 °C. Alexa Fluor donkey anti-rabbit secondary antibody (Invitrogen) was used at 1:1,000. Cell counts were performed manually using a fluorescence microscope fitted with a 20× objective.

ACKNOWLEDGMENTS. We thank Maria Esteban Lopez for help with the morphometric analysis of confocal images; Nevin Varghese for assistance with recombinant protein preparation; and Dr. Akina Hoshino for early fibrillation experiments. Human tissue was obtained from the NIH NeuroBioBank. This work was supported by NIH R21 AG045741-02 (to I.L.).

1. Valastyan JS, Lindquist S (2014) Mechanisms of protein-folding diseases at a glance. *Dis Model Mech* 7(1):9–14.
2. Eisele YS, et al. (2015) Targeting protein aggregation for the treatment of degenerative diseases. *Nat Rev Drug Discov* 14(11):759–780.
3. Hipp MS, Park SH, Hartl FU (2014) Proteostasis impairment in protein-misfolding and -aggregation diseases. *Trends Cell Biol* 24(9):506–514.
4. Lashuel HA, Overk CR, Oueslati A, Masliah E (2013) The many faces of α-synuclein: From structure and toxicity to therapeutic target. *Nat Rev Neurosci* 14(1):38–48.
5. Spillantini MG, et al. (1997) Alpha-synuclein in Lewy bodies. *Nature* 388(6645): 839–840.
6. McLean PJ, et al. (2002) TorsinA and heat shock proteins act as molecular chaperones: Suppression of alpha-synuclein aggregation. *J Neurochem* 83(4):846–854.
7. Sasaki K, Doh-ura K, Wakisaka Y, Iwaki T (2002) Clusterin/apolipoprotein J is associated with cortical Lewy bodies: Immunohistochemical study in cases with alpha-synucleinopathies. *Acta Neuropathol* 104(3):225–230.
8. Lowe J, et al. (1992) alpha B crystallin expression in non-lenticular tissues and selective presence in ubiquitinated inclusion bodies in human disease. *J Pathol* 166(1):61–68.
9. Sun Y, MacRae TH (2005) Small heat shock proteins: Molecular structure and chaperone function. *Cell Mol Life Sci* 62(21):2460–2476.
10. Kim YE, Hipp MS, Bracher A, Hayer-Hartl M, Hartl FU (2013) Molecular chaperone functions in protein folding and proteostasis. *Annu Rev Biochem* 82:323–355.
11. Schneider JL, Cuervo AM (2013) Chaperone-mediated autophagy: Dedicated saviour and unfortunate victim in the neurodegeneration arena. *Biochem Soc Trans* 41(6): 1483–1488.
12. Carman A, Kishinevsky S, Koren J, 3rd, Lou W, Chiosis G (2013) Chaperone-dependent neurodegeneration: A molecular perspective on therapeutic intervention. *J Alzheimers Dis Parkinsonism* 2013(Suppl 10):2013.
13. Doyle SM, Genest O, Wickner S (2013) Protein rescue from aggregates by powerful molecular chaperone machines. *Nat Rev Mol Cell Biol* 14(10):617–629.
14. Fricker LD, et al. (2000) Identification and characterization of proSAAS, a granin-like neuroendocrine peptide precursor that inhibits prohormone processing. *J Neurosci* 20(2):639–648.
15. Sayah M, Fortenberry Y, Cameron A, Lindberg I (2001) Tissue distribution and processing of proSAAS by proprotein convertases. *J Neurochem* 76(6):1833–1841.
16. Mzhavia N, et al. (2002) Processing of proSAAS in neuroendocrine cell lines. *Biochem J* 361(Pt 1):67–76.
17. Gomes I, et al. (2013) GPR171 is a hypothalamic G protein-coupled receptor for BigLEN, a neuropeptide involved in feeding. *Proc Natl Acad Sci USA* 110(40):16211–16216.
18. Gomes I, et al. (2016) Identification of GPR83 as the receptor for the neuroendocrine peptide PEN. *Sci Signal* 9(425):ra43.
19. Feng Y, Reznik SE, Fricker LD (2001) Distribution of proSAAS-derived peptides in rat neuroendocrine tissues. *Neuroscience* 105(2):469–478.
20. Morgan DJ, et al. (2005) Embryonic gene expression and pro-protein processing of proSAAS during rodent development. *J Neurochem* 93(6):1454–1462.
21. Lanoue E, Day R (2001) Coexpression of proprotein convertase SPC3 and the neuroendocrine precursor proSAAS. *Endocrinology* 142(9):4141–4149.
22. Kudo H, et al. (2009) Identification of proSAAS homologs in lower vertebrates: Conservation of hydrophobic helices and convertase-inhibiting sequences. *Endocrinology* 150(3):1393–1399.
23. Qian Y, et al. (2000) The C-terminal region of proSAAS is a potent inhibitor of prohormone convertase 1. *J Biol Chem* 275(31):23596–23601.
24. Cameron A, Fortenberry Y, Lindberg I (2000) The SAAS granin exhibits structural and functional homology to 7B2 and contains a highly potent hexapeptide inhibitor of PC1. *FEBS Lett* 473(2):135–138.
25. Morgan DJ, et al. (2010) The propeptide precursor proSAAS is involved in fetal neuropeptide processing and body weight regulation. *J Neurochem* 113(5):1275–1284.
26. Alarcon C, Verchere CB, Rhodes CJ (2012) Translational control of glucose-induced islet amyloid polypeptide production in pancreatic islets. *Endocrinology* 153(5):2082–2087.
27. Kikuchi K, et al. (2003) An N-terminal fragment of ProSAAS (a granin-like neuroendocrine peptide precursor) is associated with tau inclusions in Pick's disease. *Biochem Biophys Res Commun* 308(3):646–654.
28. Wada M, et al. (2004) A human granin-like neuroendocrine peptide precursor (proSAAS) immunoreactivity in tau inclusions of Alzheimer's disease and parkinsonism-dementia complex on Guam. *Neurosci Lett* 356(1):49–52.
29. Abdi F, et al. (2006) Detection of biomarkers with a multiplex quantitative proteomic platform in cerebrospinal fluid of patients with neurodegenerative disorders. *J Alzheimers Dis* 9(3):293–348.
30. Finehout EJ, Franck Z, Choe LH, Relkin N, Lee KH (2007) Cerebrospinal fluid proteomic biomarkers for Alzheimer's disease. *Ann Neurol* 61(2):120–129.
31. Jahn H, et al. (2011) Peptide fingerprinting of Alzheimer's disease in cerebrospinal fluid: Identification and prospective evaluation of new synaptic biomarkers. *PLoS One* 6(10):e26540.
32. Davidsson P, et al. (2002) Studies of the pathophysiological mechanisms in frontotemporal dementia by proteome analysis of CSF proteins. *Brain Res Mol Brain Res* 109(1-2):128–133.
33. Hoshino A, et al. (2014) A novel function for proSAAS as an amyloid anti-aggregant in Alzheimer's disease. *J Neurochem* 128(3):419–430.
34. Biancalana M, Koide S (2010) Molecular mechanism of Thioflavin-T binding to amyloid fibrils. *Biochim Biophys Acta* 1804(7):1405–1412.
35. Moussaud S, et al. (2015) Targeting α-synuclein oligomers by protein-fragment complementation for drug discovery in synucleinopathies. *Expert Opin Ther Targets* 19(5):589–603.
36. Roberts RF, Wade-Martins R, Alegre-Abarrategui J (2015) Direct visualization of alpha-synuclein oligomers reveals previously undetected pathology in Parkinson's disease brain. *Brain* 138(Pt 6):1642–1657.
37. Kerppola TK (2006) Visualization of molecular interactions by fluorescence complementation. *Nat Rev Mol Cell Biol* 7(6):449–456.
38. Xie HR, Hu LS, Li GY (2010) SH-SY5Y human neuroblastoma cell line: In vitro cell model of dopaminergic neurons in Parkinson's disease. *Chin Med J (Engl)* 123(8):1086–1092.
39. Danzer KM, et al. (2011) Heat-shock protein 70 modulates toxic extracellular α-synuclein oligomers and rescues trans-synaptic toxicity. *FASEB J* 25(1):326–336.
40. Helwig M, et al. (2013) The neuroendocrine protein 7B2 suppresses the aggregation of neurodegenerative disease-related proteins. *J Biol Chem* 288(2):1114–1124.

41. Bobkova NV, et al. (2014) Therapeutic effect of exogenous hsp70 in mouse models of Alzheimer's disease. *J Alzheimers Dis* 38(2):425–435.
42. Saxena S, Caroni P (2011) Selective neuronal vulnerability in neurodegenerative diseases: From stressor thresholds to degeneration. *Neuron* 71(1):35–48.
43. Peinado JR, Sami F, Rajpurohit N, Lindberg I (2013) Blockade of islet amyloid polypeptide fibrillation and cytotoxicity by the secretory chaperones 7B2 and proSAAS. *FEBS Lett* 587(21):3406–3411.
44. Dedmon MM, Christodoulou J, Wilson MR, Dobson CM (2005) Heat shock protein 70 inhibits alpha-synuclein fibril formation via preferential binding to prefibrillar species. *J Biol Chem* 280(15):14733–14740.
45. Huang C, et al. (2006) Heat shock protein 70 inhibits alpha-synuclein fibril formation via interactions with diverse intermediates. *J Mol Biol* 364(3):323–336.
46. Chorell E, et al. (2015) Bacterial chaperones CsgE and CsgC differentially modulate human α-synuclein amyloid formation via transient contacts. *PLoS One* 10(10):e0140194.
47. Hilton GR, Lioe H, Stengel F, Baldwin AJ, Benesch JL (2013) Small heat-shock proteins: Paramedics of the cell. *Top Curr Chem* 328:69–98.
48. Mzhavia N, Berman Y, Che FY, Fricker LD, Devi LA (2001) ProSAAS processing in mouse brain and pituitary. *J Biol Chem* 276(9):6207–6213.
49. Snead D, Eliezer D (2014) Alpha-synuclein function and dysfunction on cellular membranes. *Exp Neurobiol* 23(4):292–313.
50. El-Agnaf OM, et al. (2003) Alpha-synuclein implicated in Parkinson's disease is present in extracellular biological fluids, including human plasma. *FASEB J* 17(13):1945–1947.
51. Borghi R, et al. (2000) Full length alpha-synuclein is present in cerebrospinal fluid from Parkinson's disease and normal subjects. *Neurosci Lett* 287(1):65–67.
52. Tokuda T, et al. (2006) Decreased alpha-synuclein in cerebrospinal fluid of aged individuals and subjects with Parkinson's disease. *Biochem Biophys Res Commun* 349(1): 162–166.
53. Lee PH, et al. (2006) The plasma alpha-synuclein levels in patients with Parkinson's disease and multiple system atrophy. *J Neural Transm (Vienna)* 113(10):1435–1439.
54. Jang A, et al. (2010) Non-classical exocytosis of alpha-synuclein is sensitive to folding states and promoted under stress conditions. *J Neurochem* 113(5):1263–1274.
55. Emmanouilidou E, et al. (2010) Cell-produced alpha-synuclein is secreted in a calcium-dependent manner by exosomes and impacts neuronal survival. *J Neurosci* 30(20): 6838–6851.
56. Lee HJ, Patel S, Lee SJ (2005) Intravesicular localization and exocytosis of alpha-synuclein and its aggregates. *J Neurosci* 25(25):6016–6024.
57. Emmanouilidou E, et al. (2011) Assessment of α-synuclein secretion in mouse and human brain parenchyma. *PLoS One* 6(7):e22225.
58. Sung JY, et al. (2001) Induction of neuronal cell death by Rab5A-dependent endocytosis of alpha-synuclein. *J Biol Chem* 276(29):27441–27448.
59. Hansen C, et al. (2011) α-Synuclein propagates from mouse brain to grafted dopaminergic neurons and seeds aggregation in cultured human cells. *J Clin Invest* 121(2): 715–725.
60. Lotharius J, Brundin P (2002) Pathogenesis of Parkinson's disease: Dopamine, vesicles and alpha-synuclein. *Nat Rev Neurosci* 3(12):932–942.
61. Winner B, et al. (2011) In vivo demonstration that alpha-synuclein oligomers are toxic. *Proc Natl Acad Sci USA* 108(10):4194–4199.
62. Danzer KM, et al. (2007) Different species of alpha-synuclein oligomers induce calcium influx and seeding. *J Neurosci* 27(34):9220–9232.
63. Hsu LJ, et al. (2000) alpha-synuclein promotes mitochondrial deficit and oxidative stress. *Am J Pathol* 157(2):401–410.
64. Cooper AA, et al. (2006) Alpha-synuclein blocks ER-Golgi traffic and Rab1 rescues neuron loss in Parkinson's models. *Science* 313(5785):324–328.
65. Freeman D, et al. (2013) Alpha-synuclein induces lysosomal rupture and cathepsin dependent reactive oxygen species following endocytosis. *PLoS One* 8(4):e62143.
66. Winslow AR, et al. (2010) α-Synuclein impairs macroautophagy: Implications for Parkinson's disease. *J Cell Biol* 190(6):1023–1037.
67. Snyder H, et al. (2003) Aggregated and monomeric alpha-synuclein bind to the S6′ proteasomal protein and inhibit proteasomal function. *J Biol Chem* 278(14):11753–11759.
68. Esteban-Martín S, Silvestre-Ryan J, Bertoncini CW, Salvatella X (2013) Identification of fibril-like tertiary contacts in soluble monomeric α-synuclein. *Biophys J* 105(5):1192–1198.
69. Emadi S, Barkhordarian H, Wang MS, Schulz P, Sierks MR (2007) Isolation of a human single chain antibody fragment against oligomeric alpha-synuclein that inhibits aggregation and prevents alpha-synuclein-induced toxicity. *J Mol Biol* 368(4):1132–1144.
70. Huang C, Ren G, Zhou H, Wang CC (2005) A new method for purification of recombinant human alpha-synuclein in *Escherichia coli*. *Protein Expr Purif* 42(1):173–177.
71. Guest PC, et al. (2002) Proinsulin processing in the diabetic Goto-Kakizaki rat. *J Endocrinol* 175(3):637–647.
72. Croisier E, et al. (2006) Comparative study of commercially available anti-alpha-synuclein antibodies. *Neuropathol Appl Neurobiol* 32(3):351–356.
73. Hawrylycz MJ, et al. (2012) An anatomically comprehensive atlas of the adult human brain transcriptome. *Nature* 489(7416):391–399.
74. Gray H, Clemente CD (1985) *Anatomy of the Human Body* (Lea & Febiger, Philadelphia), 30th Ed, p 1676.
75. Danzer KM, et al. (2012) Exosomal cell-to-cell transmission of alpha synuclein oligomers. *Mol Neurodegener* 7:42.
76. Sulzer D, et al. (1992) Weak base model of amphetamine action. *Ann N Y Acad Sci* 654:525–528.